Effect of morphology on the crack propagation of the semicrystalline polyester poly(1,4-dimethylene-*trans*-cyclohexyl suberate)

J. M. Pochan, W. F. Parsons and J. F. Elman
Research Laboratories, Eastman Kodak Company, Rochester, NY 14650, USA
(Received 20 May 1983)

Crack propagation of the semicrystalline polymer poly(1,4-dimethylene-*trans*-cyclohexyl suberate) (MCS) was studied as a function of polymer morphology. MCS was characterized in terms of degree of crystallinity and crystal growth kinetics. Spherulitic band size and radius show similar temperature dependencies. The energy to propagate a crack was correlated with spherulitic radius for a low-molecular-weight material (M_n=24 500). Brittle fracture occurs in this material with little large-scale plastic deformation. What plastic deformation there is, however, correlated with spherulitic band orientation. A higher-molecular-weight sample (M_n=38 000) shows plastic deformation over the entire temperature range studied. Energy to fracture agrees with a modified Griffith criterion in which the characteristic dimension is spherulitic radius. Annealing experiments show that energy to fracture is controlled by lamellar thickness, decreasing with increasing thickness. Fracture morphology shows little interspherulitic failure, with intraspherulitic failure (low-molecular-weight material) or plastic deformation (high-molecular-weight material) being the prevalent modes.

(Keywords: crack; propagation; polymer; semicrystalline; morphology; hot melt)

INTRODUCTION

The study of fracture in polymers has become increasingly important with the advent of their use as engineering materials. Several studies have been done on amorphous and crystalline materials[1-3] but relatively few on semicrystalline polymers[4-8].

The influence of morphology (spherulitic size, lamellar thickness) on the mechanical properties of semicrystalline polymers has long been recognized. Friedrich recently reported the effect of morphology on fracture in polypropylene[4,9]. He studied three basic morphologies, fine spherulites, coarse spherulites in a fine spherulitic matrix, and fully grown coarse spherulites, and showed that fracture depended on (1) spherulitic size, (2) strain rate and (3) molecular weight, with resistance to crack propagation being a decreasing linear function of spherulitic size, a decreasing function of strain rate and an increasing function of molecular weight. Within a given molecular-weight series, the stress intensity factor for a single-edge-cracked plate under tension[1]

$$K_I = \sigma_0 \sqrt{(\pi a)} f(a/b)$$

(where σ_0 is the stress at crack propagation, a is the initial crack length, and $f(a/b)$ is a correction factor derived for certain specimen dimensions and crack configurations[10,11]) increased as the spherulitic size decreased. In the small-spherulite samples, crack propagation was controlled by a craze formation in front of the crack tip, whereas in the large-spherulite samples the fracture propagated along the spherulite boundaries. This latter effect was attributed to the weakening of the interspherulite region due to rejection of non-crystallizable low-molecular-weight components.

In those studies the effect of lamellar thickness and annealing of the semicrystalline material was not described. In our work, crack-propagation studies on the semicrystalline polyester poly(1,4-dimethylene-*trans*-cyclohexyl suberate) (MCS) (*Figure 1*) include the effect of thermal history. We also present crystal-growth and crack-morphology studies.

EXPERIMENTAL

Sample preparation

The MCS was prepared in house; its characterization is shown in *Table 1*. Crack-propagation samples were prepared in Teflon moulds $10 \times 1 \times 0.32$ cm^3. Polymer samples were melted into the moulds at 413K in 10^{-3} mmHg vacuum. The samples were then either quenched in a water bath or placed immediately in an annealing oven at the annealing temperature desired. The quenched samples were transferred to an oven at the same temperature and annealed for 21 h. Cracks were placed in the sample either by a razor-blade notch or by inserting a piece of Teflon-coated Kapton into the sample during the forming phase. A 0.5 cm crack was used in all samples. All

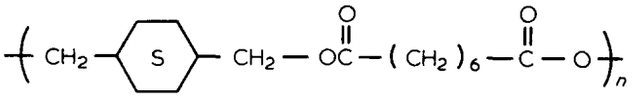

Figure 1 Structure of poly(1,4-dimethylene-*trans*-cyclohexyl suberate) (MCS)

0032-3861/84/071031-09$03.00

Table 1 Characterization of poly(1,4-dimethylene-*trans*-cyclohexyl suberate)

Sample designation	M_n*	M_w*	M_w/M_n
MSC-I	24 770	48 050	1.94
MCS-II	38 000	77 500	2.04
MCS-III	29 000	59 600	2.06
MCS-IV	34 800	69 900	2.01
MCS-V	39 600	78 000	1.97
MCS-VI	42 800	110 500	2.58
MCS-VII	39 500	90 300	2.29

* Polystyrene equivalent molecular weight

crack-propagation studies were done with samples MCS-I and MCS-II at room temperature. Size-exclusion chromatography experiments run before and after moulding showed that, within the limits of measurement error, no degradation occurred.

Small-angle light scattering (SALS)

SALS experiments to obtain average spherulitic size and banding structure were done in a standard fashion[12,13]. Samples for the SALS experiments were made by subjecting thin samples ($\sim 100\ \mu m$) melted onto glass slide covers to identical thermal conditions as the crack-propagation samples. From the cloverleaf H_v SALS patterns, the average spherulite size was calculated from the formula of Stein and Rhodes[12].

$$\sin\left(\frac{\theta}{2}\right)=\frac{\lambda}{\pi R} \quad (1)$$

where R is the spherulite radius, λ is the wavelength of incident light and θ is the scattering angle.

Microscopy and crystal growth rate studies

An Olympus Vanox microscope with attached Mettler FP52 temperature stage was used for optical microscopy. Crystal growth was studied by cooling samples melted onto microscope slides to a specific annealing temperature in the Mettler stage and then photographing the result as a function of time. The growth rates were obtained by comparing the micrographs with a stage micrometer. At fast nucleation and growth rates, a photocell was installed in the exposure meter port of the microscope, and birefringence was monitored as a function of time. The slope of the curve of photocell output vs. time was compared directly with growth rate at higher temperature (slower rates); a linear correlation existed. These photocell data were thus used to extend the experimental range of the experiments.

A Jeol JSM 35C instrument was used for scanning electron microscopy of fracture surfaces. Fractured specimens were gold-coated before examination in the secondary scanning mode.

Degree of crystallinity

The degree of crystallinity was determined by differential scanning calorimetry (d.s.c.) after the heat of fusion of a 100% crystalline material had been determined by d.s.c. measurements and a pulsed n.m.r. technique[14]. This value was 29.9 cal g^{-1}.

Mechanical testing

Mechanical testing was done on an Instron model 1113 instrument. Samples were held in pneumatic grips and tested in the tensile mode. A gauge length of 4.5 cm was used. Samples were observed with a Gaertner optical extensometer, and propagation was noted visually. The crosshead speed from these experiments was 0.2 cm min^{-1}.

Use of endplates. Endplates were used to exclude the possibility of sample slippage in the pneumatic grips because of high stresses. Aluminium plates with 90° angles (*Figure 2*) were heated to 110°C and quickly sealed to the polymer, which was at ambient temperature except in the immediate region of the bond. The sample was immediately clamped in the grips. This firmly seated the endplates while the polymer was still slightly soft and rapidly cooled them, thus minimizing heat transfer to the bulk of the sample.

Determining energy to propagate. The testpiece was positioned so that the base of the crack was initially observed, or the sample was rotated 90° so that the crack profile was observed as an opening triangle. In the first position, cavitation of samples could be observed at the crack tip when they had grown to a size that could be resolved by the 20-power optical extensometer. This point was recorded on the strip chart by an event marker. In the profile position the 'same' event could be marked, with proper illumination, as a result of the scatter produced by the cavities. All data were taken with the sample in the first position. The energy to propagate the crack is given by integrating the area under the stress–strain curve up to the event marker. In samples where no cavitation occurred, crack propagation was observed as essentially brittle fracture.

Physical characterization of MCS

Characterization involved experiments that would determine parameters of potential importance to the crack propagation of MCS. These were degree of crystallinity, crystal growth kinetics, spherulitic size and molecular weight[15].

The molecular weights of the materials used in these experiments are shown in *Table 1*. Only two samples (MCS-I and MCS-II) were used in the crack propagation studies. Zero-shear melt viscosity data (*Figure 3*) indicated that all samples were above the entanglement molecular weight.

The degree of crystallinity in general varied linearly with annealing temperature from ~40% for samples quenched and annealed at room temperature to ~48% for samples quenched and annealed near the melting point (~95°C). For sample MCS-I, the melting point was invariant, with $T_m = 97.4° \pm 0.8$°C for all samples annealed below 90°C. T_g was −20°C for all samples.

Same samples showed a small amount of material melting near 91°C under certain annealing conditions. This melting point was never the major melting peak, but could be an indication of another polymorph in the system or premelt phenomena. The melting point increased to up to 104°C at annealing temperatures of 95°C,

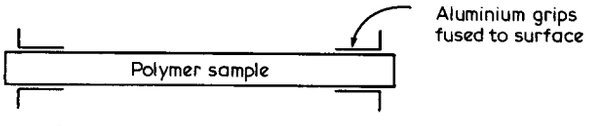

Figure 2 Sample conformation with aluminium grips

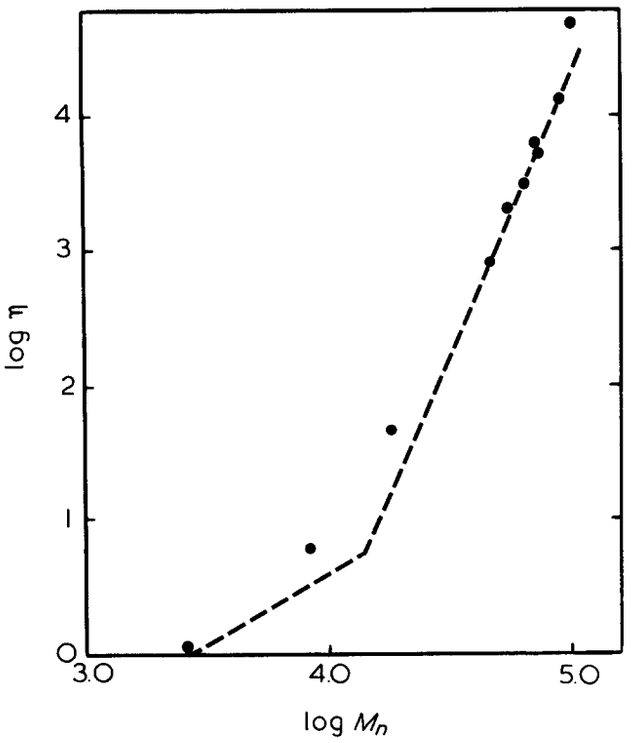

Figure 3 Log(zero-shear viscosity) vs. log M_n for MCS

which indicates a gradual increase in lamellar thickness above 90°C[15]. In MCS-II the average melting point observed for all annealing temperatures was 96.8° ± 1.2°C. The lower melting point for the higher-molecular-weight material suggests the inability of the high-molecular-weight materials to reorganize into as thick lamellae as the low-molecular-weight polymer[16].

RESULTS

Growth kinetics

To ensure that samples had crystallized within the experimental time frame, we studied the growth rates of MCS-II and MCS-I (see Experimental section). The morphology of the samples is a function of nucleation and growth, and both these processes can be described by similar equations

$$\dot{n} = n_0 T \exp(-E_d/RT) \exp(-\Delta F^*/RT) \qquad (1)$$

where $\dot{n}$ is the homogeneous nucleation or growth rate, E_d is the activation energy for viscous flow across the crystal amorphous boundary, ΔF is the free-energy change for crystallization, R is the universal gas constant, and T is the absolute temperature[17,18]. ΔF^* is a function of the degree of supercooling of the polymer melt and the shape of the crystal nucleus in the case of nucleation theory. For the cylindrical-nucleation model in which contributions from strain and edge free energies have been ignored[19], equation (1) becomes

$$\dot{n} = n_0 T \exp(-E_d/RT) \exp\left(\frac{8\pi\bar{\sigma}^3 T_m^2}{\Delta H^2 R T \Delta T^2}\right) \qquad (2)$$

where T_m is the crystal melt temperature, ΔH is the heat of fusion of the 100% crystalline material, $\bar{\sigma}$ is the average surface free energy of the crystal, and ΔT ($T_m - T$) is the degree of supercooling of the sample. Equation (2) predicts that the rate measurement will maximize at some temperature T^* and that above this temperature the rate will be controlled by the thermodynamics of crystallization and growth, i.e. the driving force to move amorphous material across the crystal/amorphous boundary. Below T^* the microviscosity of the system will dominate, i.e. although the free energy is sufficient for crystal growth, it is limited by the ability to move molecules across the crystal/amorphous interface. Normally, two parameters are obtained from equation (2), E_d and $\bar{\sigma}$, the latter provided that ΔH_f can be measured. The former is obtained from a plot of log(growth rate) vs. $1/T$, and the latter requires the high-temperature data to be replotted as log(growth rate/T) vs. $T_m^2 T^{-1} \Delta T^{-2}$. The growth rate data for MCS-I and MCS-II are shown in *Figure 4*; only data at temperatures above the rate maximum were obtained. The data show a rate maximum near 50°C; however, this cannot be quantified, as nucleation and growth in this region were too fast to obtain good data by our experimental technique. At lower temperatures down to ~0°C, the rate of formation was also too fast for accurate measurement. The samples could, however, be quenched in liquid nitrogen to an amorphous glass.

The data are not unlike those of Mandelkern[19,20] and Magill[21], showing decreased growth rates with increasing molecular weight. The ratio of rates is fairly constant at ~2 and does not scale as the ratio of M_n to the 0.5 power as was observed by Magill for silane-derivative polymers[22].

The high-temperature data in *Figure 4* were linearized by replotting them as a function of $T\Delta T^{-2}$, indicating that three-dimensional nucleation and growth are prevalent for MCS. No attempt was made to calculate $\bar{\sigma}$ as it is the cube-root average of σ_u (the lateral free surface energy of the crystal) and σ_e (the end free energy of the crystal). The value of $\bar{\sigma}^3$ derived from equation (2) was 3176 erg^3 cm^{-6}.

The growth-rate results show that, except at very high

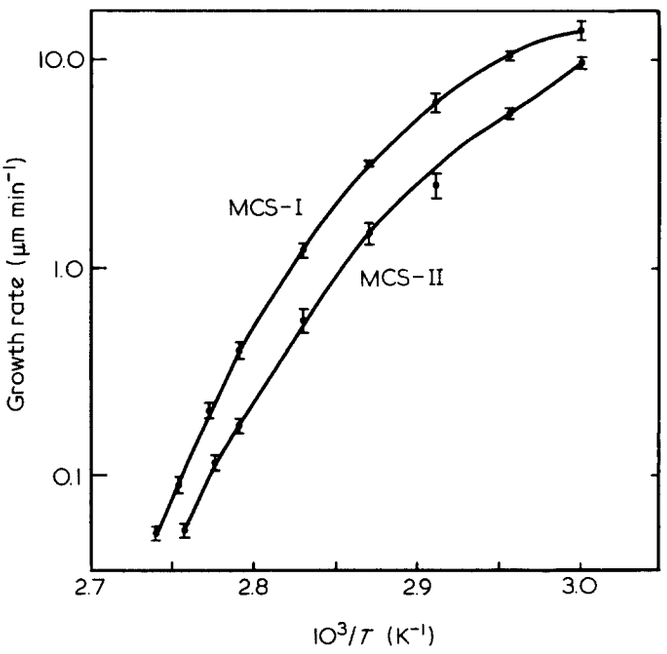

Figure 4 Log(relative crystal growth rate) vs. inverse temperature for MCS-I and MCS-II

temperatures (within a few degrees of the melting point), all samples produced for crack-propagation studies had crystallized as much as possigle and that small-angle light-scattering (SALS) data would indicate the impingement spherulite size in the sample.

Spherulitic morphology

MCS crystallizes in a banded spherulitic morphology (*Figure 5*). The spherulite size as determined by SALS is shown in *Figure 6*. The size of the spherulites varied from ~3 μm at 20°C to 300–400 μm at 90°C and provided a wide range of gross morphological character over which crack propagation could be studied. The band size was also determined by secondary light scattering[13]; *Figure 7* shows an example of the second-order scattering. *Figure 8* shows a plot of band size vs. annealing temperature. The data parallel the spherulite size study in that the higher-molecular-weight material provides a smaller band size than its low-molecular-weight counterpart for a given

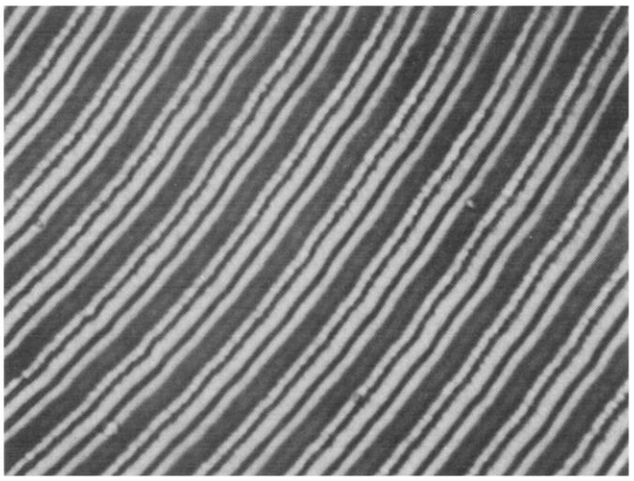

Figure 5 Banded spherulitic morphology of MCS-I. Magnification ×1000

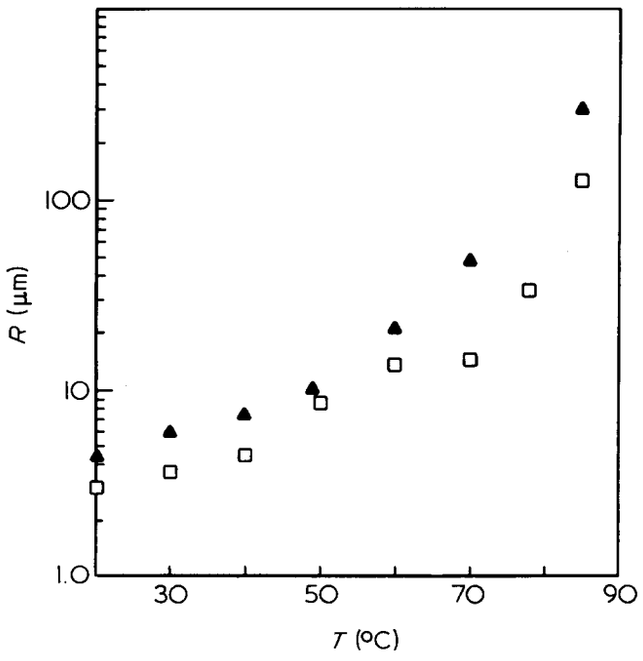

Figure 6 Spherulite radius vs. annealing temperature for MCS-I (△) and MCS-II (□)

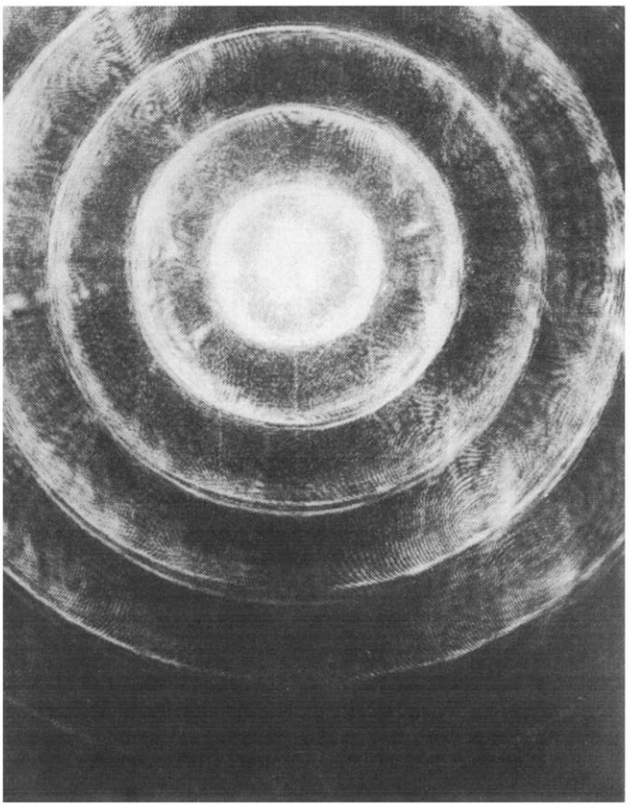

Figure 7 Second-order scattering in MCS-I. Sample annealed at 85°C

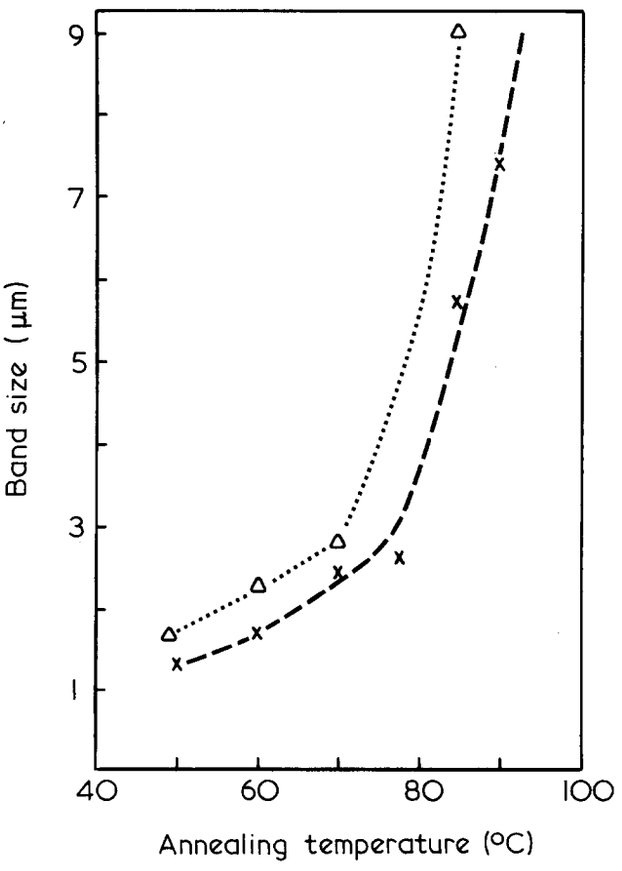

Figure 8 Band size vs. annealing temperature for MCS-I (△) and MCS-II (×)

annealing temperature. Bands in samples annealed at temperatures lower than 50°C could not be measured by the secondary scattering technique because of our experimental set-up. Both show similar temperature dependences, and in fact a plot of band size vs. spherulite size is linear, indicating that the growth kinetics are controlled similarly. The band morphology changes markedly above 85°C (*Figure 9*).

Figure 9b shows two spherulites that were nucleated and grown at 90°C. They were large and diffuse. The sample temperature was then lowered to 65°C, and the resultant increase in nucleation and decrease in band size were observed. At 95°C (*Figure 9a*), the bands were extremely diffuse. Such behaviour could be influenced by the growth kinetics and could indicate a change in nucleation and growth mechanism, such as that observed for polyethylene[23].

Mechanical properties and fracture

Modulus. The modulus of semicrystalline polymers is known to be a function of the degree of crystallinity, possibly functions of spherulitic size and lamellar thickness[24-26]. The degree of crystallinity of MCS did not vary significantly from 45% (see Physical characterization subsection) and therefore can be considered effectively constant for this analysis. Within this framework, the modulus for all samples quenched and annealed was $(3.7 \pm 0.2) \times 10^6$ N m^{-2} for MCS-I and $(3.78 \pm 0.34) \times 10^6$ N m^{-2} for MCS-II. These values were obtained for samples with ΔT ($T_m - T_{annealing}$) of 8–75K. The spherulite size varied continuously within this supercooling range (see *Figure 6*). The maximum in modulus vs. spherulitic size observed in polyethylene[27] was not observed for either MCS sample. This result could indicate that lamellar thickness did not vary significantly for these samples over the temperature range in question. There is a slight increase of modulus with increased crystallinity in MCS-II; however, the crystallinity range is small enough and measurement error large enough to make the change insignificant[26].

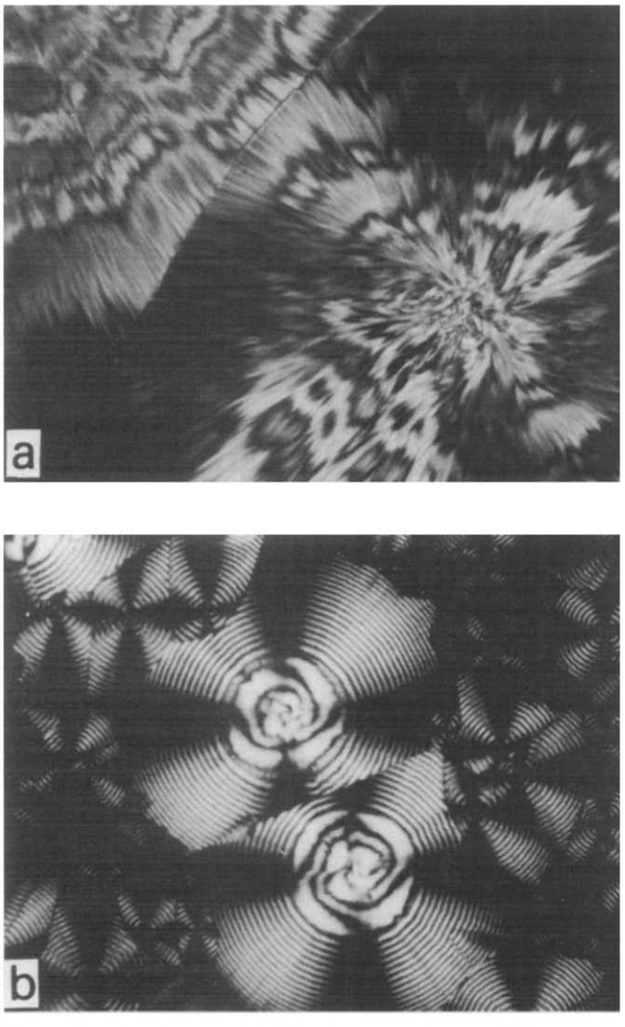

Figure 9 Morphology of MCS-I (a) crystallized at 95°C, and (b) crystallized initiall at 90°C followed by ageing at 65°C, then 55°C. Magnification?

For the experiments in which samples were slowly cooled to the annealing temperatures, the variation in modulus is much larger than the standard deviations mentioned above, with MCS-I showing similar values of modulus at ΔT of 8–20°C and lower values by 20% for a higher degree of supercooling. MCS-II slow-cooled modulus values showed similar behaviour. This result is probably due to the crystallization kinetics of the polymer. At low ΔT, results between the two general methods should be identical, as nucleation and growth are slow and the polymer reaches the equilibrium temperature before much crystallization has occurred. At higher ΔT, nucleation and growth take place at a higher temperature than the true annealing temperature, and the sample anneals significantly at the higher temperatures before it reaches thermal equilibrium. Such annealing effects have been shown to lower the modulus of the materials[27].

Crack propagation. Two parameters were measured in the crack-propagation studies, the energy to propagate (G_p) and the strain to propagate (ε_p). For the brittle samples of MCS, which behaved elastically before propagation, G_p was calculated as $\frac{1}{2}\sigma_p\varepsilon_p$, where σ_p is the stress at propagation. For samples that plastically deformed, the energy corresponds to the area under the stress–strain curve to propagation. The stress intensity factor was not calculated, as crack dimensions were uniform in all samples[1]. Because the moduli are relatively constant within these experiments, G_p can be related to the toughness of the material. *Figure 10* shows an example of the crack tip at propagation. The 'crack' starts as a fan of many small cracks, with the crack perpendicular to the stress field becoming primary as the crack progresses through the sample. These initial small cracks are similar to those observed in polypropylene (PP)[28] crack studies and are indicative of the stable crack growth region observed in PP. Similar results were obtained from cracks induced by razor notches and those from Teflon-coated Kapton inserts.

Two general types of macroscopic propagation were observed, brittle failure and plastic deformation[29]. These results correlate with molecular weight and degree of supercooling of the samples. For MCS-I, brittle failure occurred except when samples were quenched in liquid nitrogen and recrystallized at room temperature. In this case plastic deformation of the samples occurred during propagation. For MCS-II, plastic deformation and cavitation of the samples occurred during propagation over most of the annealing temperature range. At quench temperatures below 40°C, cavitation was replaced by necking and extension, with the formation of a rounded

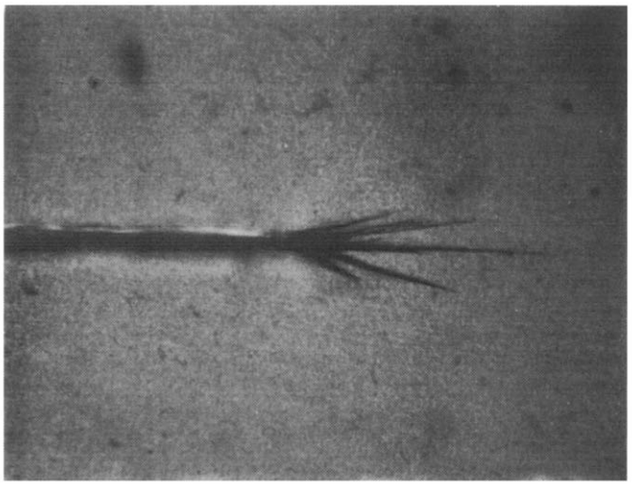

Figure 10 Photomicrograph of MCS-II sample taken after propagation observed. Magnification?

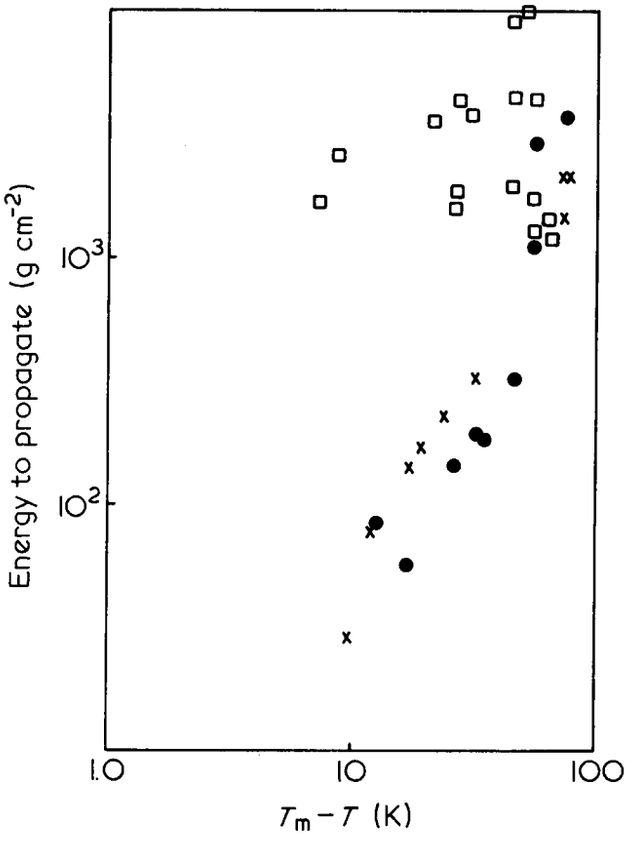

Figure 11 Energy to propagate vs. degree of supercooling for MCS-I (●=quenched sample, ×=slow cool to annealing temperature) and MCS-II (□=quenched sample)

crack tip of large radius. Failure occurred as the result of propagation of this very 'blunt' crack and appeared to be a tearing phenomenon rather than crack propagation. At 40°C, the sample would often propagate a crack but then return to a necking mode of deformation.

The higher-molecular-weight material (MCS-II) did not show as much change in G_p or ε_p with annealing as did MCS-I (*Figures 11* and *12*). For MCS-I, data for samples quenched to the annealing temperatures as well as slow cooled to the same temperature are included. For MCS-II, all slow-cooled samples had $G_p = 1842 \pm 75$ g cm^{-2} and $\varepsilon_p = 0.0033 \pm 0.0006$, an indication that morphology was controlled by nucleation and crystallization during cooling rather than by the annealing temperature.

Figures 11 and *12* show that G_p and ε_p vary significantly with the thermal conditions of preparation, with both samples showing less strength and extension to break at higher annealing temperatures, i.e. larger spherulitic sizes. The temperature dependences of quenched and slow-cooled samples of MCS-I are similar when included on the figures; however, the shape of the curves of the data obtained from the quenched samples is consistent in both thin and thick samples. The slow-cooled data will therefore be excluded from further analysis, as morphology cannot be the same as in the quenched samples.

A correlation of G_p and ε_p with molecular or morphological parameters is desired. Initially, the data in *Figures 11* and *12* were correlated with temperature functions that describe nucleation and growth data. A more satisfying correlation is shown in *Figures 13* and *14*, where G_p and ε_p are plotted vs. spherulitic radius. Except for low supercooling values, G_p for MCS-I is dependent on $R^{-1/2}$. The Griffith criterion[30] and modification of the theory, which take into account viscoelastic deformation energy[3,10,31], provide that critical stress for propagation is related to a characteristic dimension to the $\frac{1}{2}$ power. In polycrystalline ceramics, the strength of the material correlates with $d^{-1/2}$, where d is the grain size in the ceramic[32,33]. The data in *Figure 13* show that the spherulitic radius provides a possible flaw site upon which a crack can propagate. This behaviour could suggest lessening inter-spherulitic strength due to boundary impurities or lack of tie molecules between the lamellae of different spherulites. The higher G_p at small spherulite size is puzzling in that all samples were prepared similarly. It is possible that the samples still contain significant inter-lamellar tie molecules to reinforce the polymer. Schultz has shown that tie molecules between lamellae can profoundly affect the mechanical properties of semi-crystalline polymers[34]. Although there is more scatter in the data, MCS-II shows a similar spherulitic size dependence.

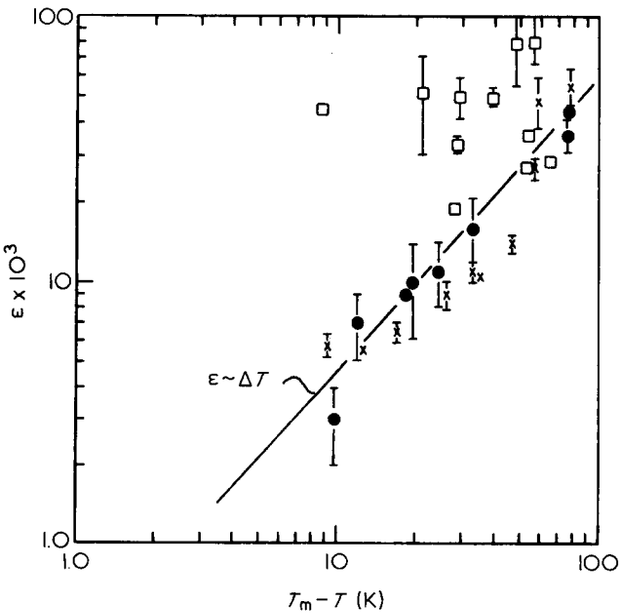

Figure 12 Strain to propagate vs. degree of supercooling for MCS-I (×=quenched sample, ●=slow cool to annealing temperature) and MCS-II (□=quenched sample)

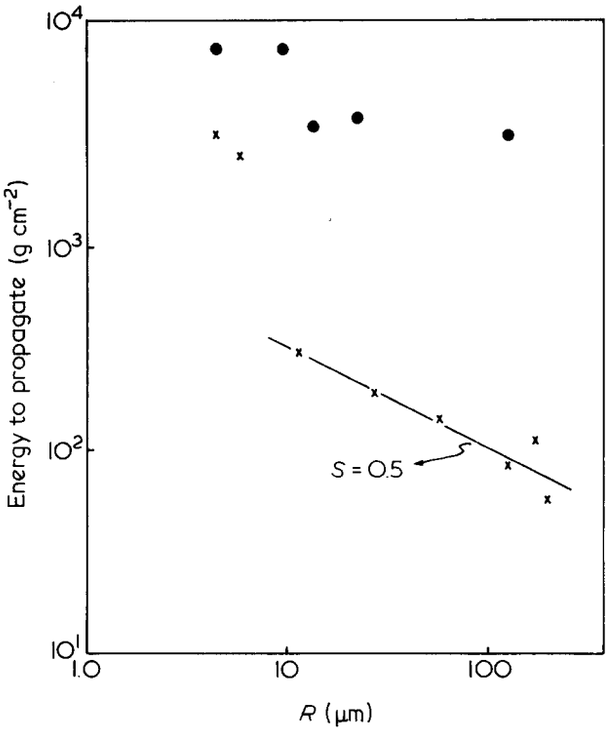

Figure 13 Energy to propagate vs. spherulitic radius for MCS-I (×) and MCS-II (●)

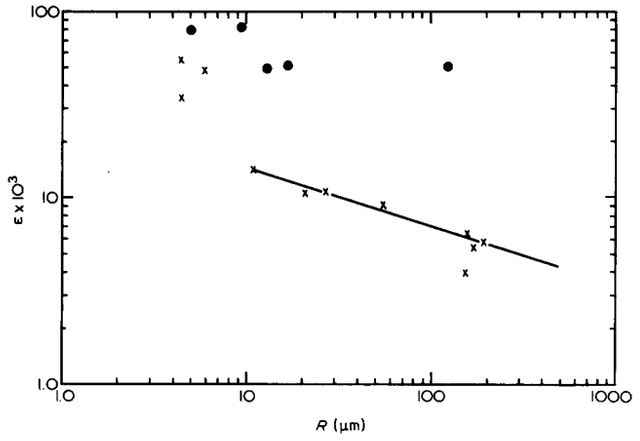

Figure 14 Strain to propagate vs. spherulitic radius for MCS-I (×) and MCS-II (●)

The ε_p data for MCS-I show a similar dependence upon the spherulitic radius (*Figure 14*). The slope, however, is less than the -0.5 measured in the G_p correlation. The values of ε_p of 1% or less for most samples show that little plastic deformation occurred before propagation. This deformation could be in the form of interlamellar tie-molecule elongation or distortion of a portion of the matrix before propagation[35]. The values of ε_p for MCS-II are nearly an order of magnitude higher than those for MCS-I and within the limited availability of data show similar spherulitic size dependence to that of MCS-I.

Annealing studies

Annealing of semicrystalline materials increases lamellar thickness and usually weakens the material[27,34]. To ascertain the effect on G_p, samples of MCS-I and MCS-II were quenched to 70°C from the melt and then annealed at various temperatures above 70°C for 21 h. The overall gross spherulite morphology of such samples does not change; however, the lamellae would be expected to thicken[36]. The results of the annealing study (*Figures 15* and *16*) show that both MCS-I and MCS-II have lower G_p as the annealing temperature is increased. The relative change for MCS-II is smaller than for MCS-I, as would be expected for the higher-molecular-weight material[16]. If the lamellar thickness is related to the annealing temperature, as has been observed previously[34], these data suggest that G_p is possibly related to lamellar thickness and to spherulitic size.

Fracture morphology

The fracture morphologies of MCS-I and MCS-II are strikingly different. Except for samples annealed above 85°C, the MCS-II samples reveal cavitation during crack propagation. An example of this cavitated surface is

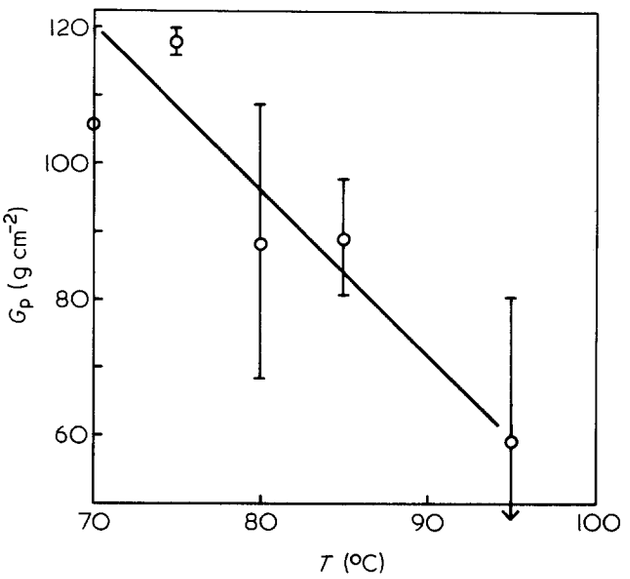

Figure 15 Energy to propagate vs. second annealing temperature for an MCS-I sample quenched to 70°C, annealed 21 h, then annealed at the specified temperature for 21 h more

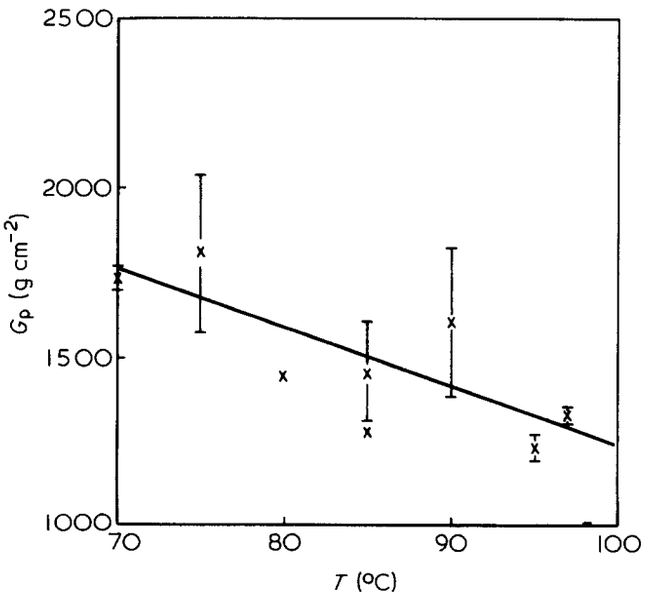

Figure 16 Energy to propagate vs. second annealing temperature for an MCS-II sample quenched at 70°C, annealed 21 h, then annealed at the specified temperature for 21 h more

shown in *Figure 17a*. The morphology resembles those observed during peel tests in which plastic deformation of the adhesive occurred and yielded very high peel forces[37]. It is obvious that large amounts of plastic deformation have taken place in the fracture surface. The high values of G_p for MCS-II are most likely due to the deformation energy required to produce this morphology. Higher-resolution photos of samples annealed at higher temperature do show cracked spherulitic morphology (*Figure 17b*). The banding structure in the spherulite is obvious and shows a change in fracture morphology along the radial direction that coincides with the band conformation.

In contrast to those of MCS-II, MCS-I fracture morphologies varied uniformly with degree of supercooling (*Figure 18*). When samples were quenched in liquid nitrogen to produce amorphous glasses, warmed slowly to 20°C and annealed at 20°C, the fracture surface of *Figure 18a* was observed. At low magnification the surface appeared smooth, and only at higher magnification could structures be observed. The small nodules in the micrograph are spherulities, and it appears as if fracture has occurred at inter-spherulitic boundaries. This morphology is similar to that observed in HDPE fractured at liquid-nitrogen temperatures but it is much more regular and in fact appears as columns of small spherulities stacked in a regular array[38]. Such a morphology was observed only when samples were made as described above. If the samples were annealed for shorter times, cavitation and plastic deformation of the fracture surface took place, suggesting that the non-equilibrium morphology (that of the growing lamellae) provided samples with either a higher amorphous content or many interlamellar tie molecules.

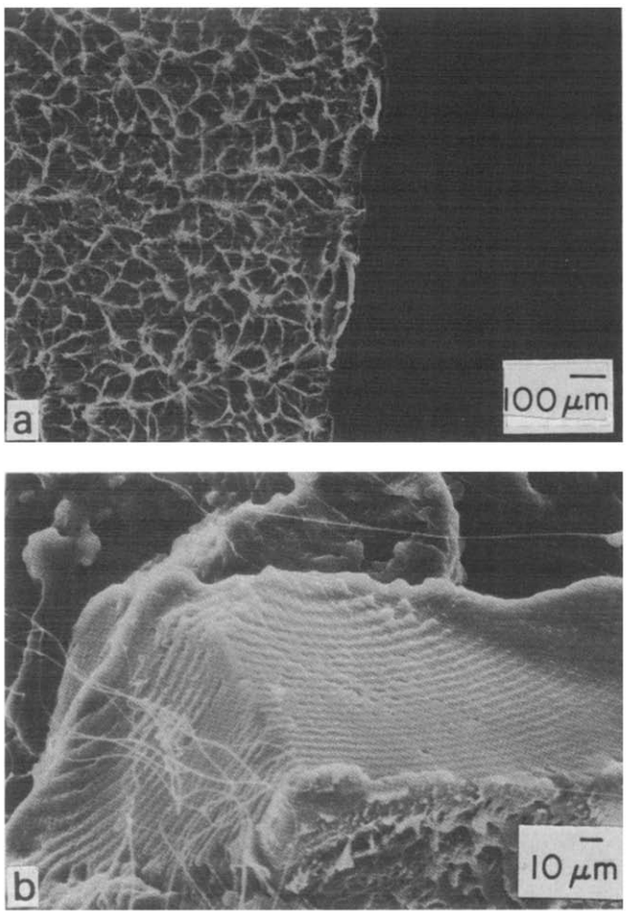

Figure 17 (a) Fracture surface of an MCS-II sample quenched to 85°C and annealed for 21 h. (b) Cracked spherulite of an MCS-II sample annealed at 90°C for 21 h

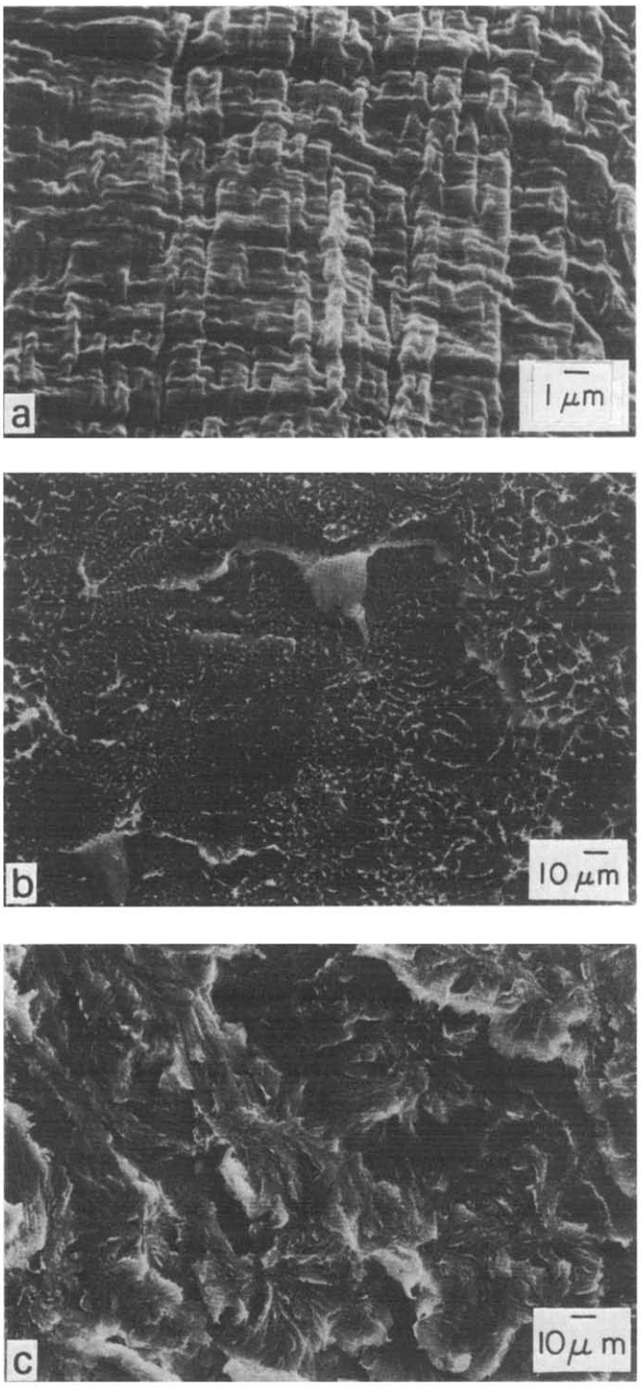

Figure 18 Fracture surface of MCS-I. Samples quenched to specified temperatures and annealed for 21 h: (a) quenched in liquid N_2–annealed at 20°C, (b) 40°C, (c) 95°C

At annealing temperatures from ambient to 85°C, fracture surfaces showed morphologies similar to those shown in *Figure 18b*. The band lines are obvious in the micrograph. Failure was trans-spherulitic with the inter-spherulitic boundary having little effect on the crack front. This is obvious from the figure, where cuts through various sections of spherulites are observed. At higher magnification (*Figure 19*) the banding is seen as localized

plastic deformation sites. As banding is thought to be twisting of the lamellar structure in the radial direction of the spherulite, this micrograph indicates the molecular orientation. If Peterlin's deformation criteria are used[39], it can be concluded that molecular chains in the lamellae are oriented parallel to the stress direction in the clean-fracture areas and perpendicular to the stress direction in the plastically deformed regions. Above 85°C, where banding becomes distorted (see *Figure 9* and text), the fracture morphology changes. The structure (see *Figure 18c*) is similar to that defined as interlamellar crack propagation in HDPE[39,40]. The surface is extremely brittle under these conditions and requires almost no energy to propagate. No evidence, except for the sample shown in *Figure 18a*, of interspherulitic fracture was observed in any of the samples.

DISCUSSION

When the above data are considered, three general findings are obtained:

(1) The molecular weight of the sample can profoundly affect the fracture of this polymer system. Although similar spherulitic sizes can be obtained for MCS-I and MCS-II, the higher-molecular-weight material deforms plastically and requires more energy to propagate a crack, whereas the low-molecular-weight material behaves brittlely and requires much less energy for crack propagation. The reason for this is most likely more interlamellar tie molecules and increased strength in the high-molecular-weight material.

(2) G_p and σ_p are a function of the spherulite size or lamellar thickness of the sample (d). The $R^{-1/2}$ dependence suggests a modified Griffith criterion for failure. A recently completed small-angle X-ray scattering study[41] of MCS-I indicates lamellar thicknesses ranging from ~130 Å for samples quenched to 20°C to 190 Å for samples formed at 90°C. These results do not provide a G_p–d correlation that is predicated on theory. The $R^{-1/2}$ dependence of G_p thus suggests an inter-spherulitic failure mechanism due to low-molecular-weight material at the spherulitic boundary. The data in *Figures 15* and *16* indicate that lamellar thickness is also important in determining the energy to propagate.

(3) Comparison of G_p or critical energy criterion to fracture morphology could be confusing. The above data suggest that the propagation energy is a function of spherulitic radius, yet morphology shows trans-spherulitic cracking with no inter-spherulitic failure. The requirements for propagation may have little to do with the observed morphology on the fracture surface.

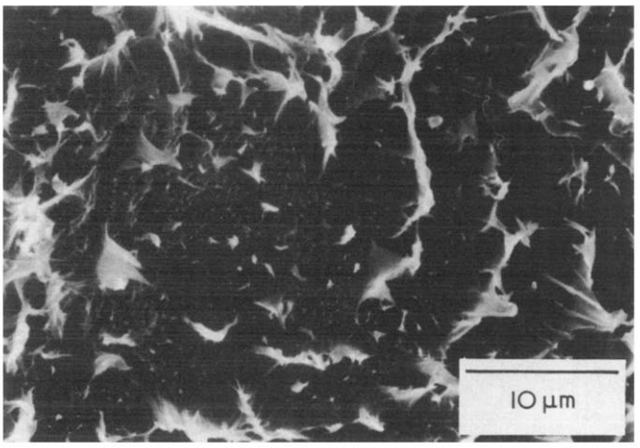

Figure 19 Fracture surface of MCS-I annealed at 40°C for 21 h

ACKNOWLEDGEMENT

We thank R. Connelly for the melt-rheology data and N. Zumbulyadis for the n.m.r. determination of the percentage crystallinity of the reference samples. The services of the Analytical Sciences Division, Kodak Research Laboratories, and the Kodak Industrial Laboratory are also acknowledged.

REFERENCES

1 Kausch, H. H. (Ed.) 'Polymer Fracture', Springer-Verlag, New York, 1978
2 Kausch, H. H., Hassell, J. A. and Jaffee, R. I. (Eds) 'Deformation and Fracture of High Polymers', Plenum Press, New York, 1972
3 Liebowitz, H. (Ed.) 'Fracture', Academic Press, New York, 1972
4 Friedrich, K. *Progr. Colloid Polym. Sci.* 1979, **66**, 299
5 Callear, J. E. and Shortall, J. B. *J. Mater. Sci.* 1972, **12**, 141
6 Way, J. L., Atkinson, J. R. and Nutting, J. *J. Mater. Sci.* 1974, **9**, 293
7 Hornbogen, E. and Friedrich, K. *J. Mater. Sci.* 1980, **15**, 2175
8 Bessel, T. J., Hull, D. and Shorthall, J. B. *J. Mater. Sci.* 1975, **10**, 1127
9 Friedrich, K. (Ed.) 'Fracture', Vol. 3, ICF4, Waterloo, Canada, 1977
10 Andrews, E. H. (Ed.) 'Fracture in Polymers', Oliver and Boyd, London, 1968
11 Dugdale, P. S. *J. Mech. Phys. Solids* 1960, **8**, 100
12 Stein, R. S. and Rhodes, M. B. *J. Appl. Phys.* 1960, **31**, 1873
13 Moore, R. S. *J. Polym. Sci. A* 1965, **3**, 4093
14 Zumbulyadis, N. private communication, Kodak Research Labs.
15 Bovey, F. and Winslow, F. (Eds) 'Macromolecules', Academic Press, New York, 1979, p. 326
16 Schultz, J. M. (Ed) 'Properties of Solid Polymeric Materials', Academic Press, New York, 1977, pp 183–90
17 Pochan, J. M. and Gibson, H. W. *J. Am. Chem. Soc.* 1972, **94**, 5573
18 Thomas, P. G. and Stavely, L. A. K. *J. Chem. Soc.* 1969, 4569
19 Mandelkern, L., Fatou, J. G. and Howard, C. *J. Phys. Chem.* 1965, **69**, 956
20 Mandelkern, L., Fatou, J. G. and Ohno, K. *J. Polym. Sci. B* 1968, **6**, 615
21 Magill, J. H. *J. Polym. Sci. B* 1968, **6**, 853
22 Magill, J. H. *J. Appl. Phys.* 1964, **35**, 3249
23 Hoffman, J. D., Davis, G. T. and Lauritzen, J. I. 'Treatise on Solid State Chemistry', Vol. 3 (Ed. N. B. Hannay), Plenum Press, New York, 1976, Chapter 7
24 Hoffman, J. D., Ross, G. S., Frolen, L. J. and Lauritzen J. Jr *J. Res. Natl Bur. Stand. A* 1975, **79**, 671
25 Nielsen, L. E. *J. Appl. Polym. Sci.* 1959, **2**, 351
26 Mohager, Y. and Wilkes, S. *J. Polym. Sci., Polym. Phys. Edn.* 1982, **20**, 457
27 Patel, J. and Phillips, P. J. *J. Polym. Sci., Polym. Lett. Edn.* 1973, **11**, 771
28 Bankert, R. J. and Takemori, M. T. IUPAC 1982 Proceedings, p 628
29 Smith, T. L. *Pure Appl. Chem.* 1970, **23**, 235
30 Griffith, A. A. *Phil. Trans. R. Soc. Lond. A* 1921, **221**, 163
31 Rivlin, R. S. and Thomas, A. G. *J. Polym. Sci.* 1953, **10**, 291
32 Bentle, G. G. and Kniefel, R. M. *J. Am. Ceram. Soc.* 1965, **48**, 570
33 Carniglia, S. C. *Mater. Sci. Res.* 1966, **3**, 425
34 Babajko, S. and Schultz, J. M. *J. Polym. Sci., Polym. Phys. Edn.* 1982, **20**, 497
35 Meinel, G. and Peterlin, A. *J. Polym. Sci. A-2* 1971, **9**, 67
36 Fischer, E. W. and Schmidt, G. F. *Angew. Chem.* 1962, **74**, 551
37 Parsons, W., Faust, M. A. and Brady, L. *J. Polym. Sci., Polym. Phys. Edn.* 1978, **16**, 775
38 Gaube, E. and Kausch, H. H. *Kuntstoffe* 1973, **63**(6), 391
39 Peterlin, A. 'Manmade Fibers: Science and Technology', Wiley, New York, 1967, p 283
40 Bandyopadhyay, S. and Brown, G. R. *Polymer* 1978, **19**, 589
41 These data provided under special contract to Eastman Kodak Company by Professor G. Wilkes and Mr S. Bagrodia, V.P.I., Blackburg, VA